JET PROPULSION LABORATORY **INTERNAL DOCUMENT**
JPL D-36832
September 22, 2006

TO: David S. Bayard (Fiscal Year 2006 R&TD on Small Body Guidance, Navigation, and Control)

FROM: John M. Carson III

SUBJECT: Small Body GN&C Research Report: G-SAMPLE - An In-Flight Dynamical Method for Identifying Sample Mass [External Release Version][1]

ABSTRACT

G-SAMPLE is an in-flight dynamical method for use by sample collection missions to identify the presence and quantity of collected sample material. The G-SAMPLE method implements a maximum-likelihood estimator to identify the collected sample mass, based on onboard force sensor measurements, thruster firings, and a dynamics model of the spacecraft. With G-SAMPLE, sample mass identification becomes a computation rather than an extra hardware requirement; the added cost of cameras or other sensors for sample mass detection is avoided. Realistic simulation examples are provided for a spacecraft configuration with a sample collection device mounted on the end of an extended boom. In one representative example, a 1000 gram sample mass is estimated to within 110 grams (95% confidence) under realistic assumptions of thruster profile error, spacecraft parameter uncertainty, and sensor noise. For convenience to future mission design, an overall sample-mass estimation error budget is developed to approximate the effect of model uncertainty, sensor noise, data rate, and thrust profile error on the expected estimate of collected sample mass.

[1] External release version of JPL Internal Document D-35998

1 Introduction

The G-SAMPLE algorithm provides a means of passively identifying collected sample mass by using the spacecraft dynamics, along with onboard sensor data collected during the ascent phase of a sample collection mission. The research conducted herein is intended to demonstrate the feasibility of utilizing sensors and dynamics models for in-flight sample-mass identification. As such, the system under study is simplified into a planar motion problem, with the model properties sized to be representative of a more-complex dynamics model.

2 Equations of Motion

2.1 Spacecraft Model

The identification algorithms are developed for a spacecraft in planar motion. The planar model used is a simplification of a representative spacecraft configuration for a sample collection mission (See figure 1). As seen in the figure, the primary spacecraft body (with mass m_{SC} and inertia I_{SC}) has two attached thrusters, along with an attached rigid boom (mass m_B, inertia I_B). The first flexible mode of the rigid boom is modeled with a rotational spring and damper. Rigidly attached to the end of the boom is a sample-collection device or end effector (mass m_{bw}, inertia I_{bw}). The sample mass (m_s), is attached to the boom/end-effector through a force sensor that allows axial translation of the sample mass along the boom longitudinal axis. The force sensor is modeled as a spring-mass-damper system with properties k_{lc}, m_{lc}, and c_{lc}, respectively.

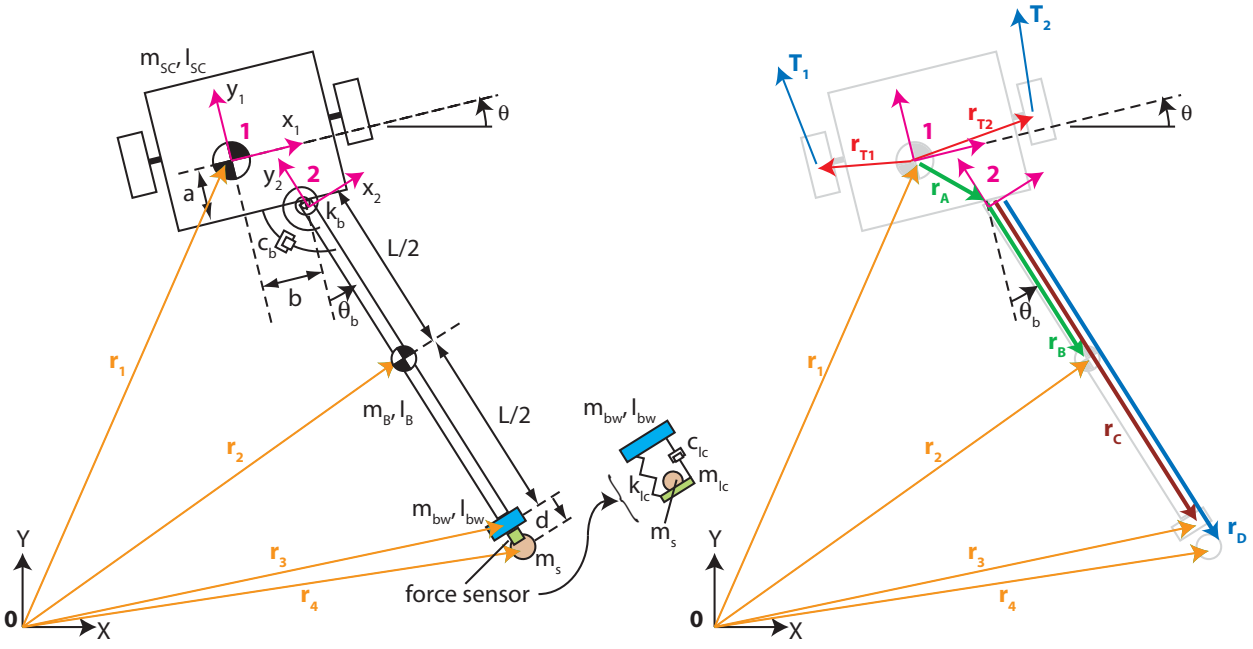

Figure 1: Spacecraft Model and Convenient Reference Frames and Relative Vectors

This multi-body dynamical system includes an offset between the spacecraft main-bus center of mass and the extended boom. Additionally, the thrust and thruster attachments are assumed

non-symmetrical with respect to the spacecraft main-bus center of mass (as represented by r_{T1}, r_{T2}, T_1, and T_2 vectors in figure 1). This model utilizes five degrees of freedom: inertial coordinates x, y, and θ, and relative coordinates θ_b and d:

$$q = (x, y, \theta, \theta_b, d)^T \tag{1}$$

Reference frame 0 in figure 1 is inertial, frame 1 is body-fixed on the spacecraft main-bus center of mass, and frame 2 is body-fixed to the boom at the spring hinge. All three frames are used to develop the multi-body dynamics. Note, the relative degree of freedom d is constrained to move axially along the boom, thus the rotation rate of the boom is identical to the rotation rate of the sample. Also, d is assumed positive in extension.

2.2 Kinematics

The kinematic relationships for the radii are as follows:

$$r_1 = \begin{pmatrix} x \\ y \end{pmatrix} \tag{2}$$

$$r_2 = r_1 + T_1^0 r_A^1 + T_2^0 r_B^2 = \begin{pmatrix} x + (b\cos\theta + a\sin\theta) + \frac{L}{2}\sin(\theta+\theta_b) \\ y + (b\sin\theta - a\cos\theta) - \frac{L}{2}\cos(\theta+\theta_b) \end{pmatrix} \tag{3}$$

$$r_3 = r_1 + T_1^0 r_A^1 + T_2^0 r_C^2 = \begin{pmatrix} x + (b\cos\theta + a\sin\theta) + L\sin(\theta+\theta_b) \\ y + (b\sin\theta - a\cos\theta) - L\cos(\theta+\theta_b) \end{pmatrix} \tag{4}$$

$$r_4 = r_1 + T_1^0 r_A^1 + T_2^0 r_D^2 = \begin{pmatrix} x + (b\cos\theta + a\sin\theta) + (L+d)\sin(\theta+\theta_b) \\ y + (b\sin\theta - a\cos\theta) - (L+d)\cos(\theta+\theta_b) \end{pmatrix} \tag{5}$$

with $r_A^1 = \begin{pmatrix} b \\ -a \end{pmatrix}$, $r_B^2 = \begin{pmatrix} 0 \\ -\frac{L}{2} \end{pmatrix}$, and $r_C^2 = \begin{pmatrix} 0 \\ -L \end{pmatrix}$, and $r_D^2 = \begin{pmatrix} 0 \\ -L-d \end{pmatrix}$. The coordinates of r_1 are in an inertial basis for frame 0, and r_2, r_3, and r_4 are all transformed into the inertial basis. Note, T_s^p represents the rotation matrix from frame s into frame p, and a superscript integer s after a vector (ex. r_B^s) indicates the vector components are written in coordinates of frame s. The expressions for the rotation matrices are as follows:

$$T_1^0 = \begin{bmatrix} \cos\theta & -\sin\theta \\ \sin\theta & \cos\theta \end{bmatrix} \tag{6}$$

$$T_2^0 = T_1^0 T_2^1 = T_1^0 \begin{bmatrix} \cos\theta_b & -\sin\theta_b \\ \sin\theta_b & \cos\theta_b \end{bmatrix} = \begin{bmatrix} \cos(\theta+\theta_b) & -\sin(\theta+\theta_b) \\ \sin(\theta+\theta_b) & \cos(\theta+\theta_b) \end{bmatrix} \tag{7}$$

The velocities associated with the four radii are

$$v_1 = \begin{pmatrix} \dot{x} \\ \dot{y} \end{pmatrix} \tag{8}$$

$$v_2 = \dot{r}_1 + T_1^0 \cancelto{0}{\dot{r}_A^1} + \widehat{\omega}_1^0 T_1^0 r_A^1 + T_2^0 \cancelto{0}{\dot{r}_B^2} + \widehat{\omega}_2^0 T_2^0 r_B^2 = \begin{pmatrix} \dot{x} - \dot{\theta}(b\sin\theta - a\cos\theta) + (\dot{\theta}+\dot{\theta}_b)\frac{L}{2}\cos(\theta+\theta_b) \\ \dot{y} + \dot{\theta}(b\cos\theta + a\sin\theta) + (\dot{\theta}+\dot{\theta}_b)\frac{L}{2}\sin(\theta+\theta_b) \end{pmatrix} \tag{9}$$

$$v_3 = \dot{r}_1 + T_1^0 \cancelto{0}{\dot{r}_A^1} + \widehat{\omega}_1^0 T_1^0 r_A^1 + T_2^0 \cancelto{0}{\dot{r}_C^2} + \widehat{\omega}_2^0 T_2^0 r_C^2 = \begin{pmatrix} \dot{x} - \dot{\theta}(b\sin\theta - a\cos\theta) + (\dot{\theta}+\dot{\theta}_b)L\cos(\theta+\theta_b) \\ \dot{y} + \dot{\theta}(b\cos\theta + a\sin\theta) + (\dot{\theta}+\dot{\theta}_b)L\sin(\theta+\theta_b) \end{pmatrix} \tag{10}$$

$$v_4 = \dot{r}_1 + T_1^0 \dot{r}_A^1 \overset{0}{\nearrow} + \widehat{\omega}_1^0 T_1^0 r_A^1 + T_2^0 \dot{r}_D^2 + \widehat{\omega}_2^0 T_2^0 r_D^2$$
$$= \begin{pmatrix} \dot{x} + \dot{d}\sin(\theta+\theta_b) - \dot{\theta}(b\sin\theta - a\cos\theta) + (\dot{\theta}+\dot{\theta}_b)(L+d)\cos(\theta+\theta_b) \\ \dot{y} - \dot{d}\cos(\theta+\theta_b) + \dot{\theta}(b\cos\theta + a\sin\theta) + (\dot{\theta}+\dot{\theta}_b)(L+d)\sin(\theta+\theta_b) \end{pmatrix} \tag{11}$$

with each velocity vector having components in an inertial basis, $\omega_1^0 = \dot{\theta}\hat{k}$, and $\omega_2^0 = (\dot{\theta}+\dot{\theta}_b)\hat{k}$. Note, $\widehat{\omega}_i^0$ is the matrix representation of the cross product operator, so

$$\widehat{\omega}_1^0 = \omega_1^0 \times (\cdot) = \begin{bmatrix} 0 & -\dot{\theta} \\ \dot{\theta} & 0 \end{bmatrix} \quad \text{and} \quad \widehat{\omega}_2^0 = \omega_2^0 \times (\cdot) = \begin{bmatrix} 0 & -(\dot{\theta}+\dot{\theta}_b) \\ (\dot{\theta}+\dot{\theta}_b) & 0 \end{bmatrix}$$

which is written in two dimensions since the system is only allowed planar motion. The expressions for v_i and ω_i^0 can be expressed in terms of the generalized coordinates of (1):

$$v_1 = B_1\dot{q}, \quad B_1 = \begin{bmatrix} 1 & 0 & 0 & 0 & 0 \\ 0 & 1 & 0 & 0 & 0 \end{bmatrix} \tag{12}$$

$$v_2 = B_2\dot{q}, \quad B_2 = \begin{bmatrix} 1 & 0 & -b\sin\theta + a\cos\theta + \frac{L}{2}\cos(\theta+\theta_b) & \frac{L}{2}\cos(\theta+\theta_b) & 0 \\ 0 & 1 & b\cos\theta + a\sin\theta + \frac{L}{2}\sin(\theta+\theta_b) & \frac{L}{2}\sin(\theta+\theta_b) & 0 \end{bmatrix} \tag{13}$$

$$v_3 = B_3\dot{q}, \quad B_3 = \begin{bmatrix} 1 & 0 & -b\sin\theta + a\cos\theta + L\cos(\theta+\theta_b) & L\cos(\theta+\theta_b) & 0 \\ 0 & 1 & b\cos\theta + a\sin\theta + L\sin(\theta+\theta_b) & L\sin(\theta+\theta_b) & 0 \end{bmatrix} \tag{14}$$

$$v_4 = B_4\dot{q}, \quad B_4 = \begin{bmatrix} 1 & 0 & -b\sin\theta + a\cos\theta + (L+d)\cos(\theta+\theta_b) & (L+d)\cos(\theta+\theta_b) & \sin(\theta+\theta_b) \\ 0 & 1 & b\cos\theta + a\sin\theta + (L+d)\sin(\theta+\theta_b) & (L+d)\sin(\theta+\theta_b) & -\cos(\theta+\theta_b) \end{bmatrix} \tag{15}$$

$$\omega_1^0 = C_1\dot{q} \quad \text{where} \qquad C_1 = \begin{bmatrix} 0 & 0 & 1 & 0 & 0 \end{bmatrix} \tag{16}$$

$$\omega_2^0 = C_2\dot{q} \quad \text{where} \qquad C_2 = \begin{bmatrix} 0 & 0 & 1 & 1 & 0 \end{bmatrix} \tag{17}$$

2.3 External and Non-Conservative Forces

The external and other non-conservative forces are added into the dynamics through the following equations [1]:

$$Q_j = \sum_{i=1}^{N_I} \left(F_i^{N_I} \cdot \gamma_{i,j} + M_i \cdot \beta_{i,j} \right) + \sum_{i=1}^{N_P} F_i^{N_P} \cdot \gamma_{i,j}^{N_P} \tag{18}$$

where N_I is the number of bodies with inertia, N_P is the number of point masses, $F_i^{N_I}$ and $F_i^{N_P}$are the external or non-conservative forces applied to the inertial bodies and point masses, respectively, M_i are the external or non-conservative moments applied to the inertial bodies, and j are the number of degrees of freedom (five in this spacecraft model, corresponding to q given in relationship (1)). Note, $\gamma_{i,j}^{N_I} = \frac{\partial r_i}{\partial q_j} = \frac{\partial v_i}{\partial \dot{q}_j}$ and $\beta_{i,j} = \frac{\partial \omega_i}{\partial \dot{q}_j}$ have r_i (absolute center-of-mass position), v_i (absolute center-of-mass velocity), and ω_i (absolute angular velocity) all referring to the i^{th} inertial body. Also, $\gamma_{i,j}^{N_P} = \frac{\partial r_i}{\partial q_j}$ has r_i referring to absolute position of the i^{th} point mass.

The sample m_s is the only point mass in the system ($N_P = 1$), and there are three inertial bodies in the model ($N_I = 3$): the main spacecraft bus, the boom, and the end effector. The

following are the external and non-conservative forces and moments:

$$F_1^{N_I} = T_1^0(T_1 + T_2) \qquad M_1 = c_b\dot{\theta}_b + r_{T1} \times T_1 + r_{T2} \times T_2 \tag{19}$$

$$F_2^{N_I} = 0 \qquad M_2 = -c_b\dot{\theta}_b \tag{20}$$

$$F_3^{N_I} = T_2^0 \begin{pmatrix} 0 \\ -c_{lc}\dot{d} \end{pmatrix} \qquad M_3 = 0 \tag{21}$$

$$F_1^{N_P} = T_2^0 \begin{pmatrix} 0 \\ c_{lc}\dot{d} \end{pmatrix} \tag{22}$$

for thrust vectors T_1 and T_2 with thruster locations r_{T1} and r_{T2}, respectively, all written in frame 1. Note, since the dynamics model is planar, the moments M_i are all positive for a counter-clockwise, in-plane rotation. For the r_i, v_i, and ω_i of the spacecraft dynamics model, the necessary $\gamma_{i,j}^{N_I}$, $\gamma_{i,j}^{N_P}$, and $\beta_{i,j}$ matrices are

$$\gamma_{1,j}^{N_I} = \left[\begin{array}{ccccc} 1 & 0 & 0 & 0 & 0 \\ 0 & 1 & 0 & 0 & 0 \end{array}\right], \tag{23}$$

$$\gamma_{3,j}^{N_I} = \left[\begin{array}{cc|c|c|c} 1 & 0 & -b\sin\theta + a\cos\theta + L\cos(\theta+\theta_b) & L\cos(\theta+\theta_b) & 0 \\ 0 & 1 & b\cos\theta + a\sin\theta + L\sin(\theta+\theta_b) & L\sin(\theta+\theta_b) & 0 \end{array}\right], \tag{24}$$

$$\beta_{1,j} = \left[\begin{array}{ccccc} 0 & 0 & 1 & 0 & 0 \end{array}\right], \tag{25}$$

$$\beta_{2,j} = \left[\begin{array}{ccccc} 0 & 0 & 1 & 1 & 0 \end{array}\right], \text{ and} \tag{26}$$

$$\gamma_{1,j}^{N_P} = \left[\begin{array}{cc|c|c|c} 1 & 0 & -b\sin\theta + a\cos\theta + (L+d)\cos(\theta+\theta_b) & (L+d)\cos(\theta+\theta_b) & \sin(\theta+\theta_b) \\ 0 & 1 & b\cos\theta + a\sin\theta + (L+d)\sin(\theta+\theta_b) & (L+d)\sin(\theta+\theta_b) & -\cos(\theta+\theta_b) \end{array}\right] \tag{27}$$

where j signifies the column number.

The resultant non-conservative-forces vector $Q = (Q_1, Q_2, Q_3, Q_4, Q_5)^T$ is

$$Q_1 = T_1^0(T_1 + T_2) \cdot \left[\begin{array}{c} 1 \\ 0 \end{array}\right] \tag{28}$$

$$Q_2 = T_1^0(T_1 + T_2) \cdot \left[\begin{array}{c} 0 \\ 1 \end{array}\right] \tag{29}$$

$$Q_3 = (r_{T1} \times T_1 + r_{T2} \times T_2) \cdot [1] \tag{30}$$

$$Q_4 = -c_b\dot{\theta}_b \cdot [1] = -c_b\dot{\theta}_b \tag{31}$$

$$Q_5 = T_2^0 \begin{pmatrix} 0 \\ c_{lc}\dot{d} \end{pmatrix} \cdot \left[\begin{array}{c} \sin(\theta+\theta_b) \\ -\cos(\theta+\theta_b) \end{array}\right] = -c_{lc}\dot{d}. \tag{32}$$

For clarity, the [1] in the above equations is the corresponding element from the appropriate $\beta_{i,j}$ matrix.

2.4 Dynamics

The multi-body dynamics model is developed based on Lagrangian mechanics [1], with the final equations having the form

$$\frac{d}{dt}\left(\frac{\partial T}{\partial \dot{q}}\right) - \frac{\partial T}{\partial q} = Q - \frac{\partial U}{\partial q}\,. \tag{33}$$

The kinetic energy for the multi-body system is

$$T = \frac{1}{2}m_{SC}v_1^T v_1 + \frac{1}{2}I_{SC}\omega_1^T\omega_1 + \frac{1}{2}m_B v_2^T v_2 + \frac{1}{2}I_B\omega_2^T\omega_2 + \frac{1}{2}m_{bw}v_3^T v_3 + \frac{1}{2}I_{bw}\omega_2^T\omega_2 + \frac{1}{2}(m_s + m_{lc})v_4^T v_4$$

which can be expressed in terms of the generalized coordinate vector q by using expressions (12)–(17):

$$\begin{aligned} T &= \frac{1}{2}\dot{q}^T \underbrace{\left[m_{SC}B_1^T B_1 + m_B B_2^T B_2 + m_{bw}B_3^T B_3 + (m_s + m_{lc})B_4^T B_4 + I_{SC}C_1^T C_1 + (I_B + I_{bw})C_2^T C_2\right]}_{M(q)}\dot{q} \\ &= \frac{1}{2}\dot{q}^T M(q)\dot{q}\,. \end{aligned} \tag{34}$$

The mass matrix $M(q)$ is configuration dependent since matrices B_2, B_3, and B_4 depend on components in q.

The potential energy of the system is

$$U = \frac{1}{2}k_b\theta_b^2 + \frac{1}{2}k_{lc}d^2 + \sum_{i=1}^{4} V_{SB}^i(s^i), \quad s^i \in \mathbb{R}^p \tag{35}$$

where k_b is the rotational spring stiffness, k_{lc} is the load-sensor stiffness, and $V^i(s^i)$ represents a gravity potential between spacecraft component i and the body it is orbiting. Note, the i components represent the primary spacecraft body, rigid boom, end effector, and sample/force-sensor mass combination. Additionally, $s^i \in \mathbb{R}^p$ indicates that the gravity potential may be expressed in a different coordinate system than the spacecraft dynamics. The assumption is made that s^i can be expressed as $s^i(q)$, thus the contribution of potential energy in the equations of motion (33) is expressed as

$$\frac{\partial U}{\partial q} = Kq + \sum_{i=1}^{4}\left(\frac{\partial s^i}{\partial q}\right)^T \frac{\partial V_{SB}(s^i)}{\partial s^i} \tag{36}$$

with $K = \begin{bmatrix} 0 & 0 & 0 & 0 & 0 \\ 0 & 0 & 0 & 0 & 0 \\ 0 & 0 & 0 & 0 & 0 \\ 0 & 0 & 0 & k_b & 0 \\ 0 & 0 & 0 & 0 & k_{lc} \end{bmatrix}$ and $\frac{\partial s^i}{\partial q} = \begin{bmatrix} \frac{\partial s_1^i}{\partial q_1} & \cdots & \frac{\partial s_1^i}{\partial q_5} \\ \vdots & \ddots & \vdots \\ \frac{\partial s_p^i}{\partial q_1} & \cdots & \frac{\partial s_p^i}{\partial q_5} \end{bmatrix}$.

Derivation of the multi-body equations of motion will make extensive use of the following identity [2]:

$$\frac{\partial}{\partial q}\left[A(q)B(q)\right] = \left(I_n \otimes A\right)\frac{\partial B}{\partial q} + \frac{\partial A}{\partial q}B, \quad q \in \mathbb{R}^n \tag{37}$$

where I_n is an $n \times n$ identity matrix,

$$\frac{\partial A}{\partial q} \equiv \begin{bmatrix} \frac{\partial A}{\partial q_1} \\ \frac{\partial A}{\partial q_2} \\ \vdots \\ \frac{\partial A}{\partial q_n} \end{bmatrix}, \tag{38}$$

and $\otimes$ represents the Kronecker Product.

The first term in (33), expressed by using the identity in (37), is

$$\begin{aligned}\frac{\partial T}{\partial \dot{q}} &= M(q)\dot{q} \\ \frac{d}{dt}\left(\frac{\partial T}{\partial \dot{q}}\right) &= M(q)\ddot{q} + \frac{d}{dt}\left[M(q)\right]\dot{q} = M(q)\ddot{q} + \left(\sum_{i=1}^{5}\frac{\partial M(q)}{\partial q_i}\dot{q}_i\right)\dot{q} \\ &= M(q)\ddot{q} + \left(\frac{\partial M}{\partial q}\right)^T\left(\dot{q}\otimes I_5\right)\dot{q} \end{aligned} \tag{39}$$

where $\frac{\partial M}{\partial q}$ is defined as in (38) with $A = M(q)$ and $n = 5$. The second term in (33) is similarly derived by using the identity in (37):

$$\begin{aligned}\frac{\partial T}{\partial q} &= \frac{1}{2}\frac{\partial}{\partial q}\left[\dot{q}^T M(q)\right]\dot{q} = \frac{1}{2}\left[\left(I_5\otimes\dot{q}^T\right)\frac{\partial M}{\partial q} + \cancelto{0}{\frac{\partial \dot{q}^T}{\partial q}}M(q)\right]\dot{q} \\ &= \frac{1}{2}\left(I_5\otimes\dot{q}^T\right)\frac{\partial M}{\partial q}\dot{q} \end{aligned} \tag{40}$$

with $\frac{\partial M}{\partial q}$ again defined as in (38). Thus, the equations of motion for the spacecraft become

$$M(q)\ddot{q} + \left[\left(\frac{\partial M}{\partial q}\right)^T\left(\dot{q}\otimes I_5\right) - \frac{1}{2}\left(I_5\otimes\dot{q}^T\right)\frac{\partial M}{\partial q}\right]\dot{q} = Q - \frac{\partial U}{\partial q}. \tag{41}$$

Matrices B_2, B_3, and B_4 are the contributors to the configuration dependence of $M(q)$, thus

$$\begin{aligned}\frac{\partial M}{\partial q} &= m_B\frac{\partial}{\partial q}(B_2^T B_2) + m_{bw}\frac{\partial}{\partial q}(B_3^T B_3) + (m_s + m_{lc})\frac{\partial}{\partial q}(B_4^T B_4) \\ &= m_B\left[(I_5\otimes B_2^T)\frac{\partial B_2}{\partial q} + \frac{\partial(B_2^T)}{\partial q}B_2\right] + m_{bw}\left[(I_5\otimes B_3^T)\frac{\partial B_3}{\partial q} + \frac{\partial(B_3^T)}{\partial q}B_3\right] \\ &\quad + (m_s + m_{lc})\left[(I_5\otimes B_4^T)\frac{\partial B_4}{\partial q} + \frac{\partial(B_4^T)}{\partial q}B_4\right] \end{aligned} \tag{42}$$

where the identity in (37) has been used. The components are then

$$\frac{\partial B_i}{\partial q} = \begin{bmatrix} 0_{2\times5} \\ 0_{2\times5} \\ A_{1,i} \\ A_{2,i} \\ A_{3,i} \end{bmatrix} \quad \text{and} \quad \frac{\partial(B_i^T)}{\partial q} = \begin{bmatrix} 0_{5\times2} \\ 0_{5\times2} \\ A_{1,i}^T \\ A_{2,i}^T \\ A_{3,i}^T \end{bmatrix}. \tag{43}$$

For $i = \{2, 3\}$, the components of $A_{1,i}$, $A_{2,i}$, and $A_{3,i}$ are as follows:

$$A_{1,i} = \left[\begin{array}{cc|c|c|c} 0 & 0 & -b\cos\theta - a\sin\theta - l_i\sin(\theta+\theta_b) & -l_i\sin(\theta+\theta_b) & 0 \\ 0 & 0 & -b\sin\theta + a\cos\theta + l_i\cos(\theta+\theta_b) & l_i\cos(\theta+\theta_b) & 0 \end{array}\right] \tag{44}$$

$$A_{2,i} = \left[\begin{array}{cc|c|c|c} 0 & 0 & -l_i\sin(\theta+\theta_b) & -l_i\sin(\theta+\theta_b) & 0 \\ 0 & 0 & l_i\cos(\theta+\theta_b) & l_i\cos(\theta+\theta_b) & 0 \end{array}\right] \tag{45}$$

$$A_{3,i} = 0_{2\times5} \tag{46}$$

where $l_i = \{\frac{L}{2}, L\}$ corresponding to $i = \{2, 3\}$, respectively. For $i = \{4\}$,

$$A_{1,4} = \left[\begin{array}{cc|c|c|c} 0 & 0 & -b\cos\theta - a\sin\theta - (L+d)\sin(\theta+\theta_b) & -(L+d)\sin(\theta+\theta_b) & \cos(\theta+\theta_b) \\ 0 & 0 & -b\sin\theta + a\cos\theta + (L+d)\cos(\theta+\theta_b) & (L+d)\cos(\theta+\theta_b) & \sin(\theta+\theta_b) \end{array}\right] \quad (47)$$

$$A_{2,4} = \left[\begin{array}{cc|c|c|c} 0 & 0 & -(L+d)\sin(\theta+\theta_b) & -(L+d)\sin(\theta+\theta_b) & \cos(\theta+\theta_b) \\ 0 & 0 & (L+d)\cos(\theta+\theta_b) & (L+d)\cos(\theta+\theta_b) & \sin(\theta+\theta_b) \end{array}\right] \quad (48)$$

$$A_{3,4} = \begin{bmatrix} 0 & 0 & \cos(\theta+\theta_b) & \cos(\theta+\theta_b) & 0 \\ 0 & 0 & \sin(\theta+\theta_b) & \sin(\theta+\theta_b) & 0 \end{bmatrix}. \quad (49)$$

Through the use of identity (37), equation (41) is now a convenient form for implementation in simulations because the Kronecker Product is a built-in function of simulation environments such as Matlab.

2.5 Conservative Forces (from Gravity Potential)

For development of G-SAMPLE, the gravity potential $V^i_{SB}(s^i)$ in equation (35) is expressed as

$$V^i_{SB}(s^i) = m_i g h_i \quad (50)$$

for each component $i = \{1, 2, 3, 4\}$ where gravity g is assumed constant and $s^i = h_i$ is the altitude above the surface. For the four components, h_i is the second component of the radius vectors in equations (2)–(5), and the m_i components are $m_1 = m_{SC}$, $m_2 = m_B$, $m_3 = m_{bw}$, and $m_4 = (m_s + m_{lc})$. The contribution of the gravity potential to the conservative forces, as expressed in equation (36), is determined as follows:

$$\frac{\partial V_{SB}(s^i)}{\partial s^i} = m_i g \quad (51)$$

since $s^i = h_i$, and

$$\frac{\partial s^1}{\partial q} = \begin{bmatrix} 0 & 1 & 0 & 0 & 0 \end{bmatrix} \quad (52)$$

$$\frac{\partial s^2}{\partial q} = \left[\begin{array}{cc|c|c|c} 0 & 1 & b\cos\theta + a\sin\theta + \frac{L}{2}\sin(\theta+\theta_b) & \frac{L}{2}\sin(\theta+\theta_b) & 0 \end{array}\right] \quad (53)$$

$$\frac{\partial s^3}{\partial q} = \left[\begin{array}{cc|c|c|c} 0 & 1 & b\cos\theta + a\sin\theta + L\sin(\theta+\theta_b) & L\sin(\theta+\theta_b) & 0 \end{array}\right] \quad (54)$$

$$\frac{\partial s^4}{\partial q} = \left[\begin{array}{cc|c|c|c} 0 & 1 & b\cos\theta + a\sin\theta + (L+d)\sin(\theta+\theta_b) & (L+d)\sin(\theta+\theta_b) & -\cos(\theta+\theta_b) \end{array}\right]. \quad (55)$$

Thus, in equation (36),

$$\sum_{i=1}^{4} \left(\frac{\partial s^i}{\partial q}\right)^T \frac{\partial V_{SB}(s^i)}{\partial s^i} = g \begin{pmatrix} 0 \\ m_{tot} \\ m_{app}(b\cos\theta + a\sin\theta) + m_{eff}\sin(\theta+\theta_b) \\ m_{eff}\sin(\theta+\theta_b) \\ -(m_s + m_{lc})\cos(\theta+\theta_b) \end{pmatrix} \quad (56)$$

where $m_{tot} = (m_{SC} + m_B + m_{bw} + m_s + m_{lc})$, $m_{app} = (m_B + m_{bw} + m_s + m_{lc})$, and $m_{eff} = (m_B\frac{L}{2} + m_{bw}L + (m_s + m_{lc})(L+d))$.

3 Sensor Models for Detecting Sample Mass

The force sensor in figure 2 is assumed to be an axially flexible component that connects the boom/end-effector to the collected sample. The force sensor is modeled as a linear spring-mass-damper system with stiffness k_{lc}, mass m_{lc}, and damping coefficient c_{lc}:

$$F_{lc} = k_{lc}d + c_{lc}\dot{d} \tag{57}$$

where positive, tensile forces measured by F_{lc} correspond to a positive extension of degree-of-freedom d. The actual metric obtained from the force sensor in this study is displacement d.

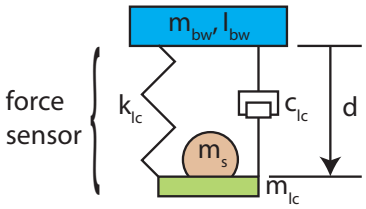

Figure 2: Force Sensor to Measure Relative Displacement d

If an accelerometer is included on the sample mass container, then the kinematic relationships in (5) are used to model the sample-mass acceleration. The inertial acceleration of the sample mass is

$$\ddot{r}_4 = \begin{pmatrix} \ddot{x} + \ddot{d}\sin(\theta+\theta_b) + \left[2\dot{d}(\dot{\theta}+\dot{\theta}_b) + (L+d)(\ddot{\theta}+\ddot{\theta}_b)\right]\cos(\theta+\theta_b) - (L+d)(\dot{\theta}+\dot{\theta}_b)^2\sin(\theta+\theta_b) \\ \ddot{y} - \ddot{d}\cos(\theta+\theta_b) + \left[2\dot{d}(\dot{\theta}+\dot{\theta}_b) + (L+d)(\ddot{\theta}+\ddot{\theta}_b)\right]\sin(\theta+\theta_b) + (L+d)(\dot{\theta}+\dot{\theta}_b)^2\cos(\theta+\theta_b) \\ -\ddot{\theta}(b\sin\theta - a\cos\theta) - \dot{\theta}^2(b\cos\theta + a\sin\theta) \\ +\ddot{\theta}(b\cos\theta + a\sin\theta) - \dot{\theta}^2(b\sin\theta - a\cos\theta) \end{pmatrix}. \tag{58}$$

Since force and acceleration measurements are along the boom axis, the acceleration of the sample mass is rotated into frame 2 (Refer back to figure 1 for a clarification of frame 2):

$$\ddot{r}_4^2 = T_0^2\ddot{r}_4$$

where $T_0^2 = (T_2^0)^T$ (Refer back to equation (7)). The sample-mass acceleration $\ddot{r}_4^2$ is a 2-element vector and contains both the axial and transverse acceleration of the sample (the axial component is the 2^{nd} element in the vector). The axial component can be related to the load sensor force F_{lc} through a simple force balance such that

$$F_{lc} = k_{lc}d + c_{lc}\dot{d} = (m_s + m_{lc})(a_{lc} + \tilde{g}) \tag{59}$$

where a_{lc} represents the 2^{nd} element of $\ddot{r}_4^2$, and $\tilde{g}$ is the contribution of gravity along the boom axis. Note, this relationship can also be used to verify that simulations are implemented correctly.

4 Sample Mass Estimator

The estimator utilized by G-SAMPLE is based on the error between force-sensor displacement measurements and displacement values expected from the force-sensor model in equation (57). The

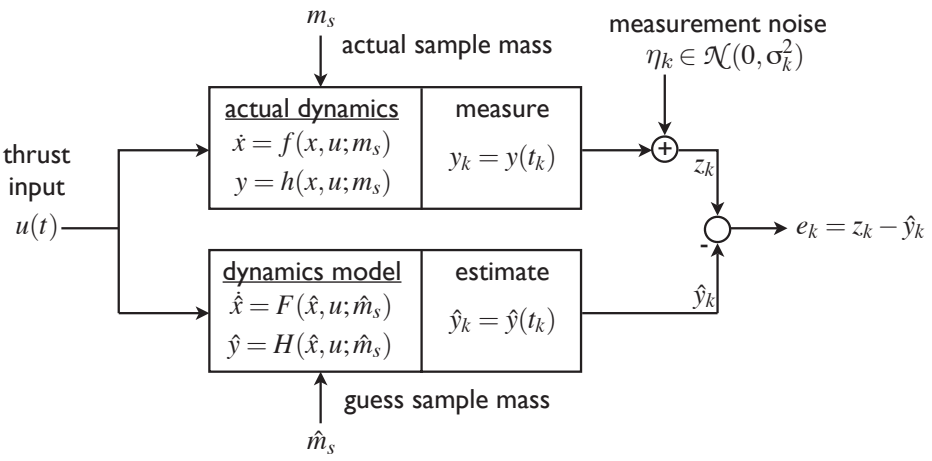

Figure 3: Measurement Versus Model for Estimator Implementation

measurement noise η_k is assumed to be white, zero-mean Gaussian noise with variance σ_k^2 and is additive to the load-sensor displacement measurement (as shown in Figure 3).

An assumption is made that the load sensor can be calibrated during a thruster-silence period prior to descent toward the surface. During this maneuver, the sample mass $m_s = 0$, and any biases in the load sensor can be characterized and removed from subsequent measurements. The 0-mean and Gaussian measurement noise $\eta_k \in \mathcal{N}(0, \sigma_k^2)$ is also assumed to have fixed variance (σ_{lc}^2) for all measurements. During the thruster-silence calibration, the measurement noise variance σ_{lc}^2 can be characterized as well.

The cost function utilized by G-SAMPLE is the summed, weighted mean-square error

$$\min_{\hat{m}_s} J = \sum_{k=1}^{N} \frac{(z_k - \hat{y}_k)^2}{\sigma_k^2} \tag{60}$$

where N is the total number of measurements, z_k is the force sensor measurement along the boom axial direction (which includes the effects of measurement noise), and $\hat{y}_k$ is the expected force sensor measurement (F_{lc}) from the guessed sample mass $\hat{m}_s$. The minimum of cost function J is found through a line search over a range of $\hat{m}_s$. This minimum corresponds to the MLE (Maximum Likelihood Estimate) of the collected sample mass, m_s^{MLE}. Confidence limits on m_s^{MLE} are obtained with

$$J(\hat{m}_s) - J(m_s^{MLE}) < q(\alpha) \tag{61}$$

where $q(\alpha)$ is the α quantile of the 1-degree-of-freedom Chi-Squared distribution. Appendix A details the derivation of cost function (60) and confidence limits (61).

5 G-SAMPLE Analysis

This section conducts in-depth analysis of G-SAMPLE. The analysis is separated into simulation, estimation, and sensitivity analyses. The simulation subsection discusses the spacecraft model and typical dynamic response characteristics, including the pure and noisy load sensor. The estimation subsection provides cost analysis based on several different collected sample masses and includes

confidence limits for different levels of sensor noise. The sensitivity subsection examines the robustness of G-SAMPLE to errors in spacecraft parameters, along with a study of the sensitivity of G-SAMPLE to errors in thrust profile.

5.1 Simulation

Simulations are based on representative parameters for a spacecraft conducting sample collection on a small celestial body (moon, asteroid, comet). See Table 1 for a listing of relevant parameters. Additionally, the thruster firing sequence utilized in the simulations is based on a representative ascent sequence where the firings are designed to keep the spacecraft orientation level (i.e. $\theta \approx 0$) during ascent.

Table 1: Simulation Parameters

parameter	**value**	**description**
m_{SC}	800 kg	spacecraft main-bus mass
I_{SC}	500 kg-m^2	spacecraft main-bus inertia
m_B	0.5 kg	flexible boom mass
I_B	0.6 kg-m^2	flexible boom inertia about boom c.m.
m_{bw}	20 kg	end-effector mass
I_{bw}	0	end-effector inertia
L	3.78 m	flexible boom length
a	0.53 m	axial offset of boom from spacecraft main-bus c.g.
b	0.53 m	lateral offset of boom from spacecraft main-bus c.g.
T_{max}	22 N	max. thrust from 45° canted thrusters, 2 per side
f_1	0.16 Hz	fundamental flexible mode frequency
ζ_1	0.001	fundamental flexible mode damping
$m_s^{desired}$	0.5 kg	desired amount of sample mass to collect

The position of the thrusters is as follows:

$$r_{T1} = \begin{pmatrix} -0.9367 \\ -0.545 \end{pmatrix} \text{m} \quad \text{and} \quad r_{T2} = \begin{pmatrix} 0.9367 \\ -0.545 \end{pmatrix} \text{m} \tag{62}$$

where r_{T1} and r_{T2} are specified in coordinates of the main spacecraft bus (frame 1).

The boom-hinge spring constant k_b in the dynamics (and as shown in figure 1) is based on the fundamental flexible mode (f_1) of a representative spacecraft/boom combination:

$$k_b = \omega_1^2 \frac{I_{SC} \cdot I_{boom}}{I_{SC} + I_{boom}} \tag{63}$$

where $\omega_1 = 2\pi f_1$, and I_{boom} is the moment of inertia about the spring hinge for the combination of the flexible boom and the end effector:

$$I_{boom} = \frac{1}{3} m_B L^2 + m_{bw} L^2. \tag{64}$$

The boom-hinge damping c_b is based on the following equation:

$$c_b = 2\zeta_1 \omega_1 \frac{I_{SC} \cdot I_{boom}}{I_{SC} + I_{boom}} \tag{65}$$

where ζ_1 is the damping coefficient chosen for the fundamental mode.

The load sensor is designed such that the unloaded frequency of sensor oscillation is 20 Hz, while the loaded (with sample mass) frequency is in the range of 10-20 Hz. The chosen point design for the load sensor has the mass, spring, and damping coefficients as provided in Table 2.

Table 2: Load-Sensor Parameters

parameter	**value**	**description**
m_{lc}	$0.625/(2\pi)^2$ kg	load-sensor mass
k_{lc}	$250\frac{\text{N}}{\text{m}}$	load-sensor stiffness
c_{lc}	$2.8135\frac{\text{kg}}{\text{sec}}$	load-sensor damping

Simulations were run for several different sample mass values in order to assess the capability of G-SAMPLE to identify the amount of sample mass collected. The response characteristics of the dynamic states are summarized well by figure 4, which is for a collected sample mass of $m_s = 1.02$ kg. The other dynamic responses are qualitatively similar and are not shown.

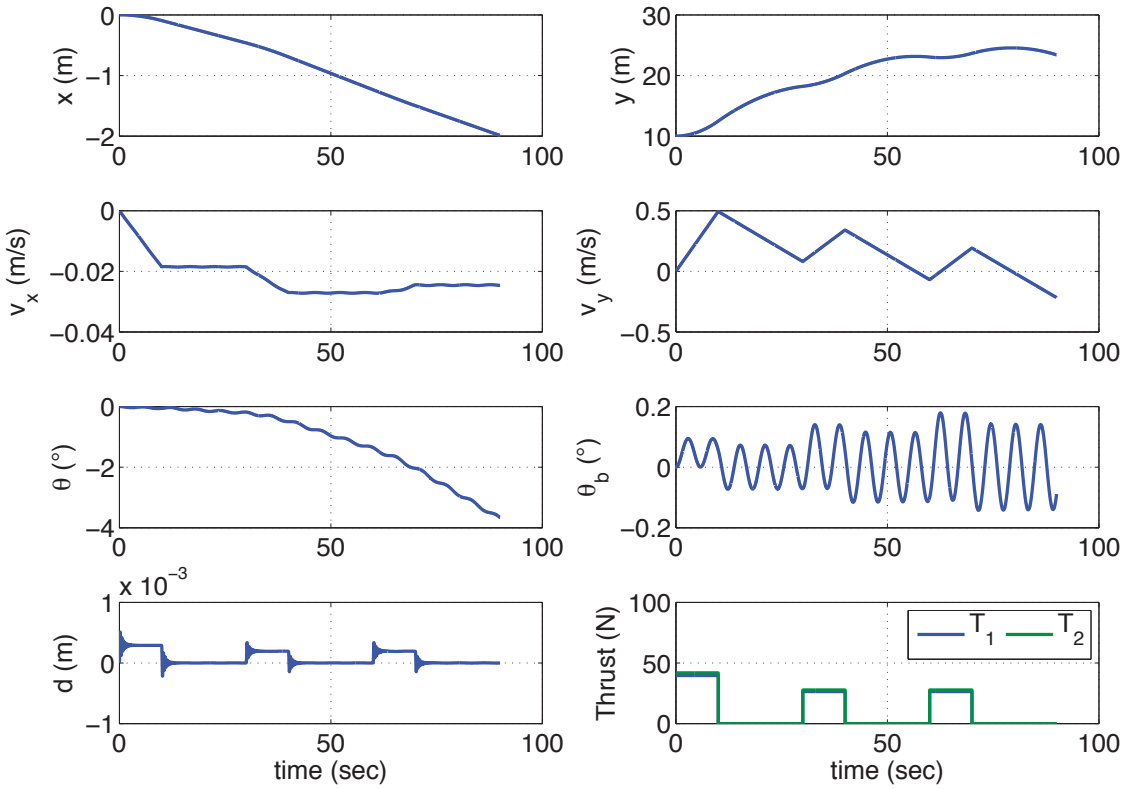

Figure 4: Typical Dynamics Response of Spacecraft (Example with $m_s = 1.02$ kg)

The responses in figure 4 provide the x and y position and velocity, the orientation θ of the main spacecraft bus, the relative orientation of the boom θ_b, the displacement d of the load sensor (without noise), and the left and right thruster magnitudes. The simulation runs for 90 seconds with the three thruster firings again representing a typical ascent scenario. The spacecraft is kept

within a 4° attitude of level during the ascent, and the altitude y increased from 10 m to 25 m. This profile was used for testing the capability of G-SAMPLE.

The load-sensor noise is additive, as discussed with figure 3. A load sensor noise floor of 50 μm (i.e. $\sigma_{lc}^2 = (5 \times 10^{-5})^2$ m^2) is used in simulations; this value also accounts for quantization error that would affect a sensor measurement. A typical sensor response is depicted in figure 5, where the load sensor displacement corresponds to that in figure 4.

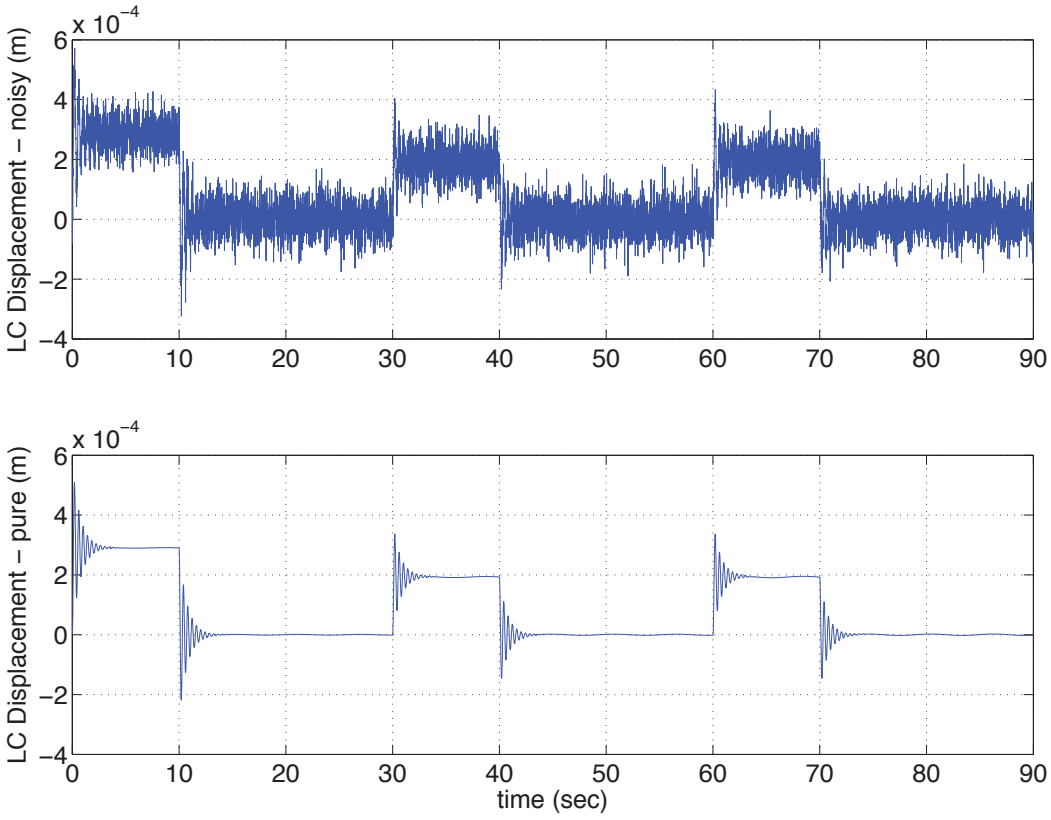

Figure 5: Typical Load-Sensor Response with Additive Noise ($\sigma_{lc} = 5 \times 10^{-5}$ m)

5.2 Estimation

For the estimation, data from the actual system (figure 4) is sampled at 50 Hz, providing 4500 samples over the 90 second ascent scenario. The line search over guesses $\hat{m}_s$ to minimize the cost function J in (60) and estimate the collected sample mass requires system simulations for each $\hat{m}_s$. These simulations each generate 4500 expected response samples and can be computationally time consuming if the line-search increment in $\hat{m}_s$ values is small. To aid in this search, a course mess is generated around the desired sample mass ($m_s^{desired} = 0.5$ kg as listed in Table 1). A step size of 0.1 kg is used with $\hat{m}_s = \{0, 0.1, 0.2, ..., 1.4, 1.5\}$ kg in the initial course mesh.

Once an initial minimum cost J is found with the course mesh, a quadratic curve is fit around this course minimum J and a better estimate of the actual minimum J^{fit} is found. The sample mass $\hat{m}_s^{fit}$ corresponding to the fit minimum J^{fit} is then run through simulations and is added to the cost curve for J. A second quadratic fit around the new data point provides a better estimate of the

actual minimum cost and associated sample mass. This form of iteration to find the true J^{MLE} and m_s^{MLE} is known as Brent's Method in one dimension [3]. Additional iteration with Brent's Method can be utilized to improve the estimate of m_s^{MLE}, but simulations with G-SAMPLE indicate that one iteration is sufficient for sample mass identification.

Figure 6 provides an example of iterating for m_s^{MLE} with Brent's Method. The estimate of m_s^{MLE} is used in the confidence limit calculations from equation (61), and the confidence limits are indicated under the bottom plot. In this particular example, a lower noise floor of 5 μm is used because the resultant parabolic cost curve has a large magnitude variation and provides a better illustration of applying Brent's Method.

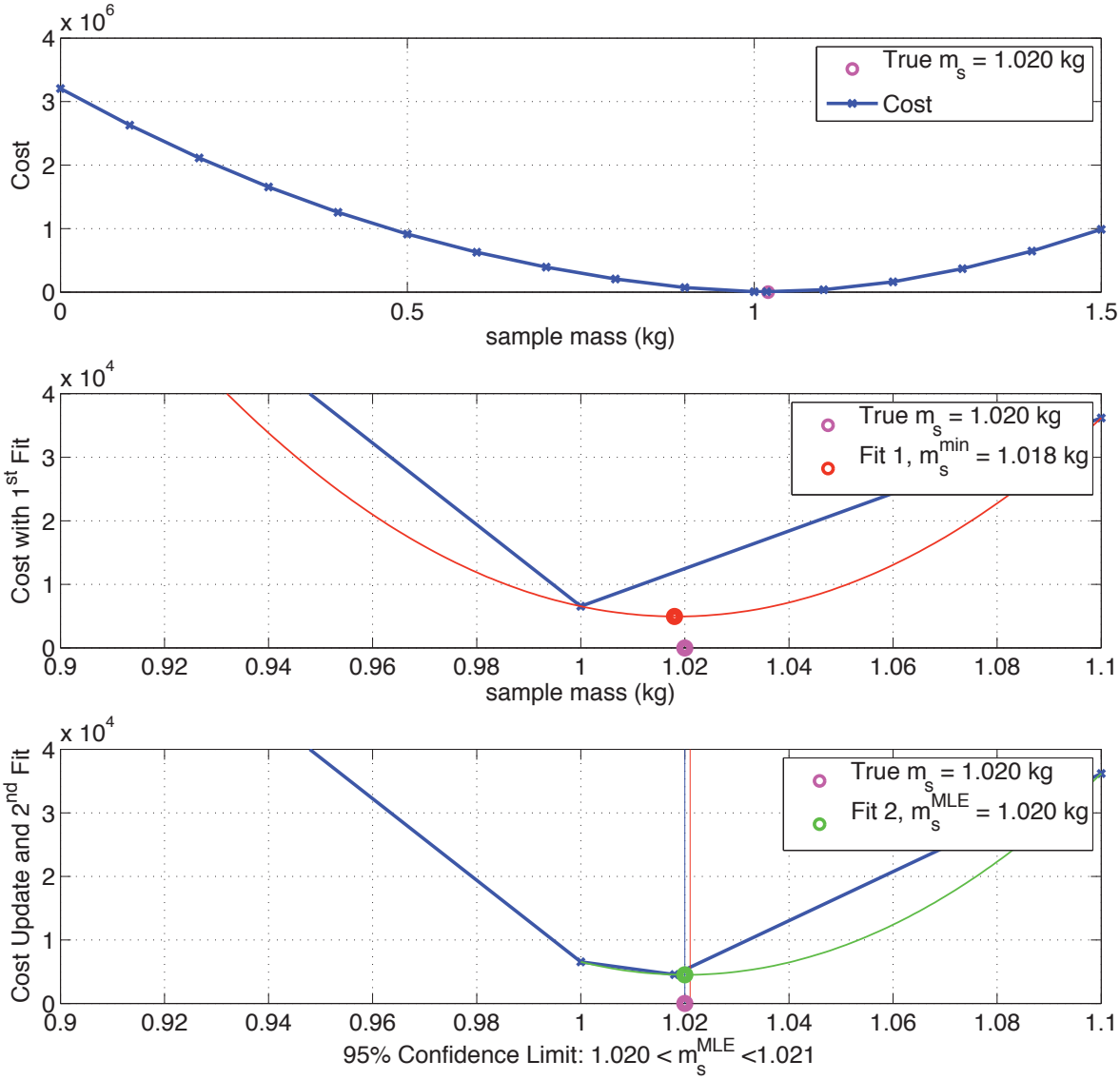

Figure 6: Utilizing Brent's Method to Determine m_s^{MLE} (cost zoomed at minimum)

The top plot in figure 6 shows the coarse cost function, which is quadratic in form. The middle

plot is a zoom of the first fit with the J^{fit} and its $\hat{m}_s^{min}$ point indicated. The bottom plot is a zoom of the refined cost function incorporating the new data point (i.e. a new simulation with a guess mass of $\hat{m}_s^{min}$), and the second fit provides m_s^{MLE}. Note, the confidence bounds included in the bottom plot of figure 6 overlap the actual collected sample mass.

The following figure (figure 7) provides the cost and confidence bounds generated by G-SAMPLE for actual collected sample masses of $m_s = \{0.53, 0.78, 1.02\}$ kg. In all cases, the m_s^{MLE} is within 10 grams of the actual collected sample and at or within the 95% confidence limits of the estimate. The noise floor of 50 μm is utilized with all the sensor measurements in these G-SAMPLE simulations, and the same thrust profile, as depicted in figure 4, is used throughout them. Note that G-SAMPLE is able to identify

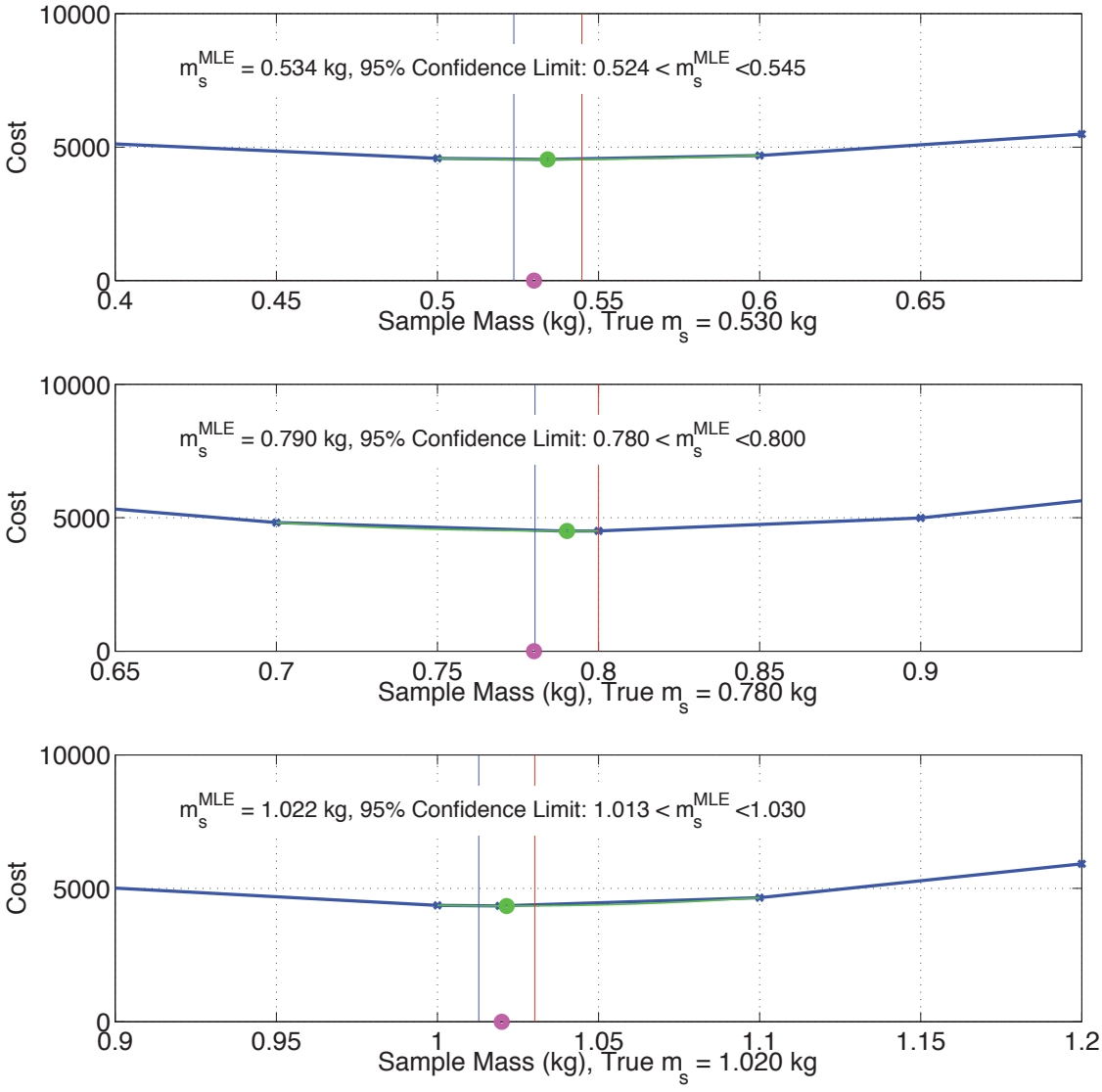

Figure 7: Estimate Comparison for Different Collected Sample Masses (costs zoomed at minimum)

A comparison simulation with a larger noise floor of 500 μm was conducted to establish the

sensitivity of the confidence limits and estimate of m_s^{MLE} to noise. Figure 8 illustrates the larger 95% confidence limits on m_s^{MLE} when a large noise floor affects the load sensor; the limits still contain the actual mass of collected sample are the width of the limits are 0.1 kg. Note, the response dynamics is figures 4 and 5 were used in this simulation with the noise floor added onto the distance d response.

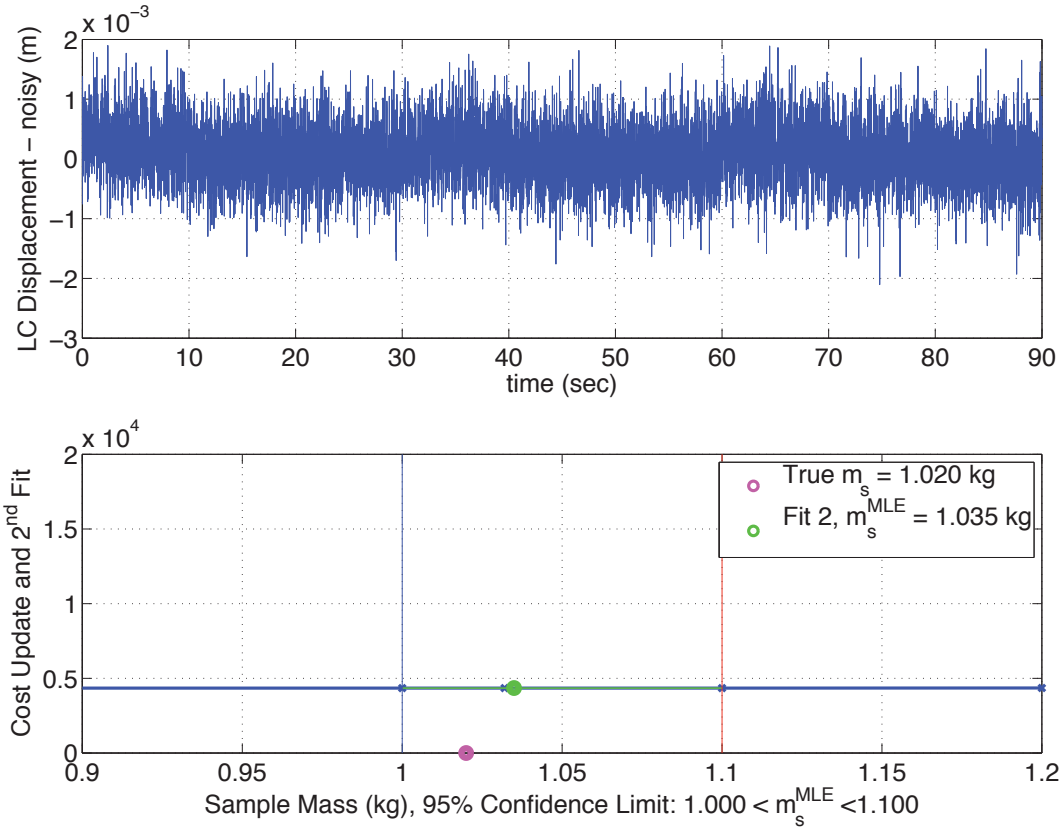

Figure 8: Confidence Limits with Larger Noise Floor of 500 μm (cost zoomed at minimum)

5.3 Sensitivity

The robustness of the G-SAMPLE method is examined by assuming knowledge error in the actual spacecraft parameters. Parameters such as inertias, center-of-mass offset, and first flexible-mode frequency and damping will not be known precisely for a spacecraft. The following parameters listed in Table 3 were perturbed from the *model* data in Table 1 for different quantities of collected sample mass: inertias are assumed known to within 10% and center-of-mass offset and first-flexible-mode parameters are assumed known to within 5%.

For a simulation of the actual system based on the perturbed parameters in Table 3, the G-SAMPLE method is capable of estimating the collected sample to within 95% confidence limits. The cost function, confidence limits, and m_s^{MLE} are shown in figure 9 for this perturbed case with a sample mass of $m_s = 1.02$ kg.

Table 3: Knowledge Error in Actual-System Parameters

parameter	value	description
I_{SC}	90% I_{SC}^{model}	spacecraft main-bus inertia
I_B	90% I_B^{model}	flexible boom inertia about boom c.m.
a	95% a^{model}	axial offset of boom from spacecraft main-bus c.g.
b	95% b^{model}	lateral offset of boom from spacecraft main-bus c.g.
k_b	95% k_b^{model}	based on k_b from equation (63)
c_b	95% c_b^{model}	based on c_b from equation (65)

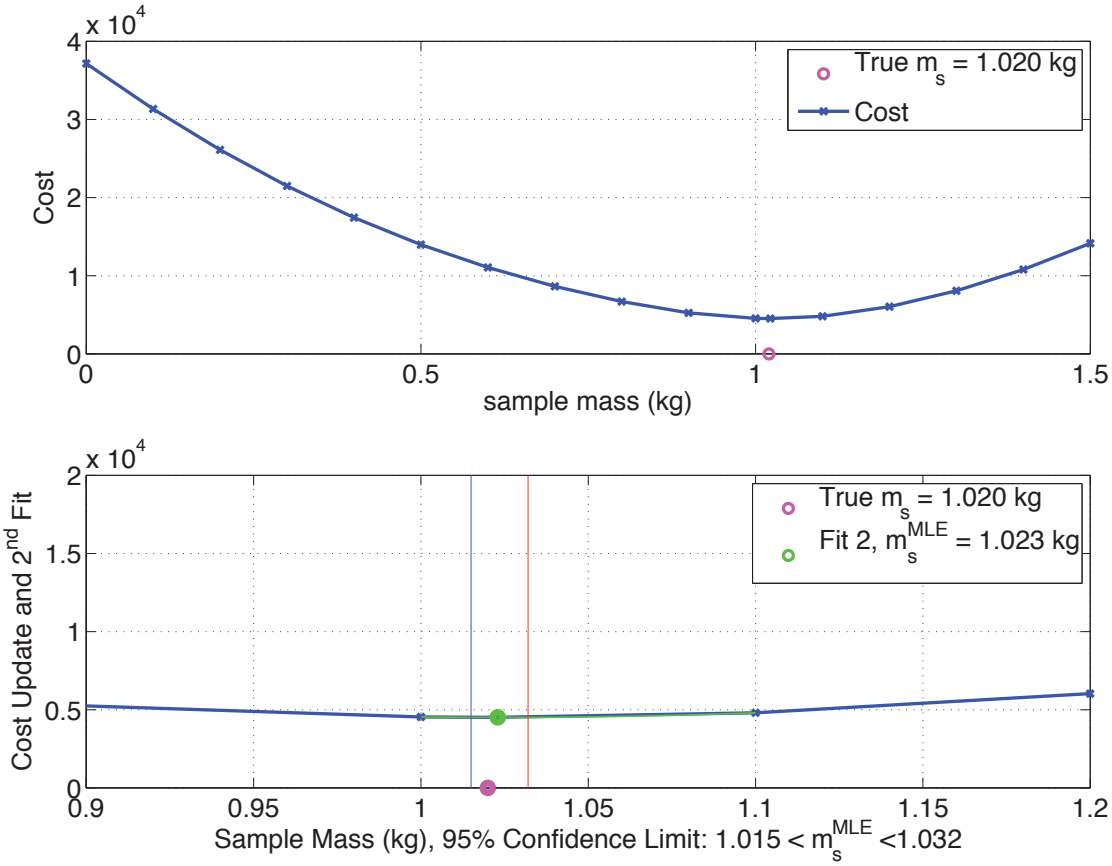

Figure 9: Estimate of Sample Mass with Knowledge Error in Actual-System Parameters

The deviation of the m_s^{MLE} between figure 9 and the bottom plot in figure 7 is only 1 gram, with the confidence limits shifts by only 2 grams. Taking the inertia errors to be 110% of the *model* and center-of-mass offset and first-flexible-mode parameters to be 105% of the *model* as in 1, the difference in m_s^{MLE} and the confidence limits is negligible (data not shown). Additionally, the small influence of errors in these model parameter holds true for other sample mass quantities too with a similar error in the parameters of Table 3.

Another relevant and significant source of sensitivity in G-SAMPLE comes from the accuracy to which thrust profiles are known. A sensitivity study was conducted for actual thruster firing

magnitudes being ±10% and ±20% off of expected values. In this study, only the thruster magnitudes are perturbed while all other parameters are assumed to be perfectly known; sensor noise of 50 μm is still included. Figure 10 illustrates the cost function and m_s^{MLE} from and estimation where actual thruster firings are 10% less than expected values.

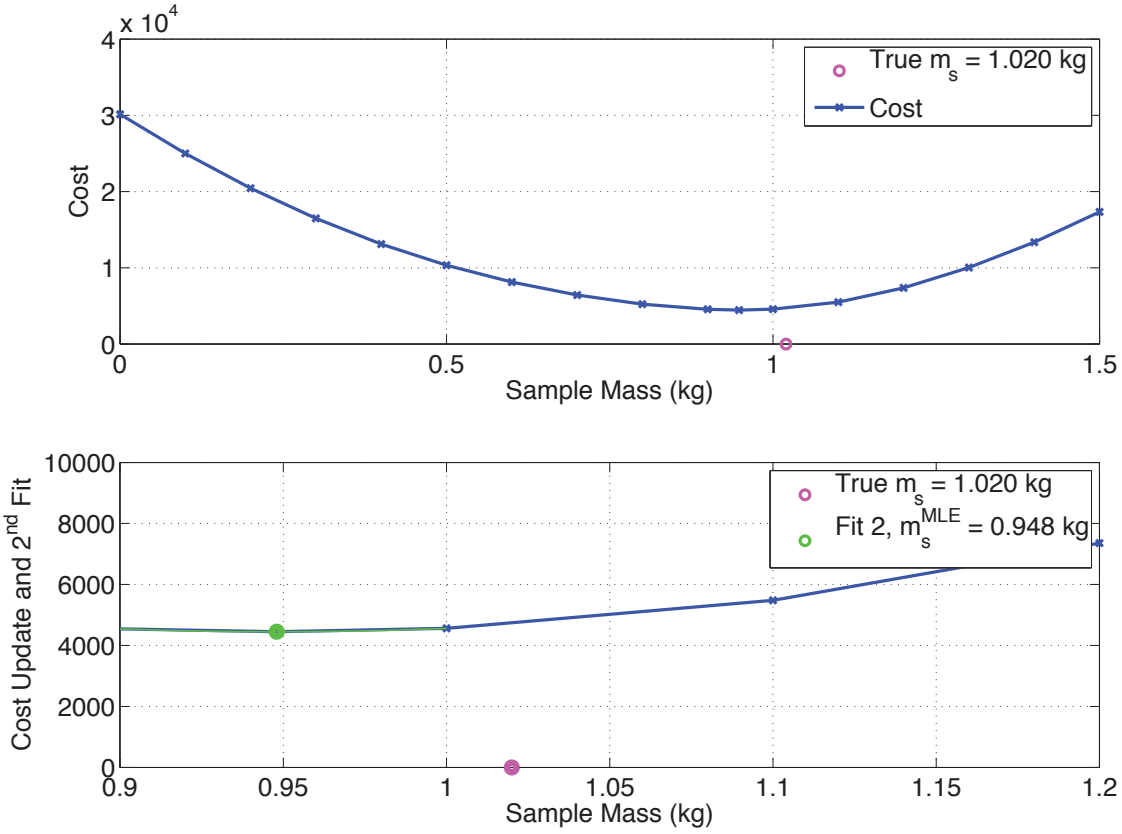

Figure 10: Cost and m_s^{MLE} Sensitivity to 10% Error in Actual Thrust Magnitude

Figure 10 indicates that for a 10% error in actual thrust, the m_s^{MLE} is off from the actual collected sample mass by approximately 10%; the confidence limits are not shown (they are incorrect) because they are based on a single-parameter model with only m_s unknown. In fact, when thrust is deviated by 20%, the m_s^{MLE} is also off from the actual sample mass by approximately 20%. The error scaling appears nearly linear.

To more accurately estimate the collected sample mass, a different estimator could be constructed to use onboard accelerometer data to better profile actual thrust. Otherwise, a separate estimation could be run before G-SAMPLE to use onboard accelerometer and other measurements to more closely identify the actual thrust, or prior to sample collection the thrusters could be more-accurately profiled with onboard accelerometer measurements.

Figure 11 contrasts four plots of the m_s^{MLE} found for the system with $m_s = 1.02$ kg and different sources of error. The first plot only contains the sensor noise, the second plot is both sensor noise and actual-parameter error, the third plot is only thrust error, and the bottom plot is a combination of all three. Notice that the difference between the third and four plots is minimal, indicating that sensitivity of G-SAMPLE is dominated by thrust profile knowledge.

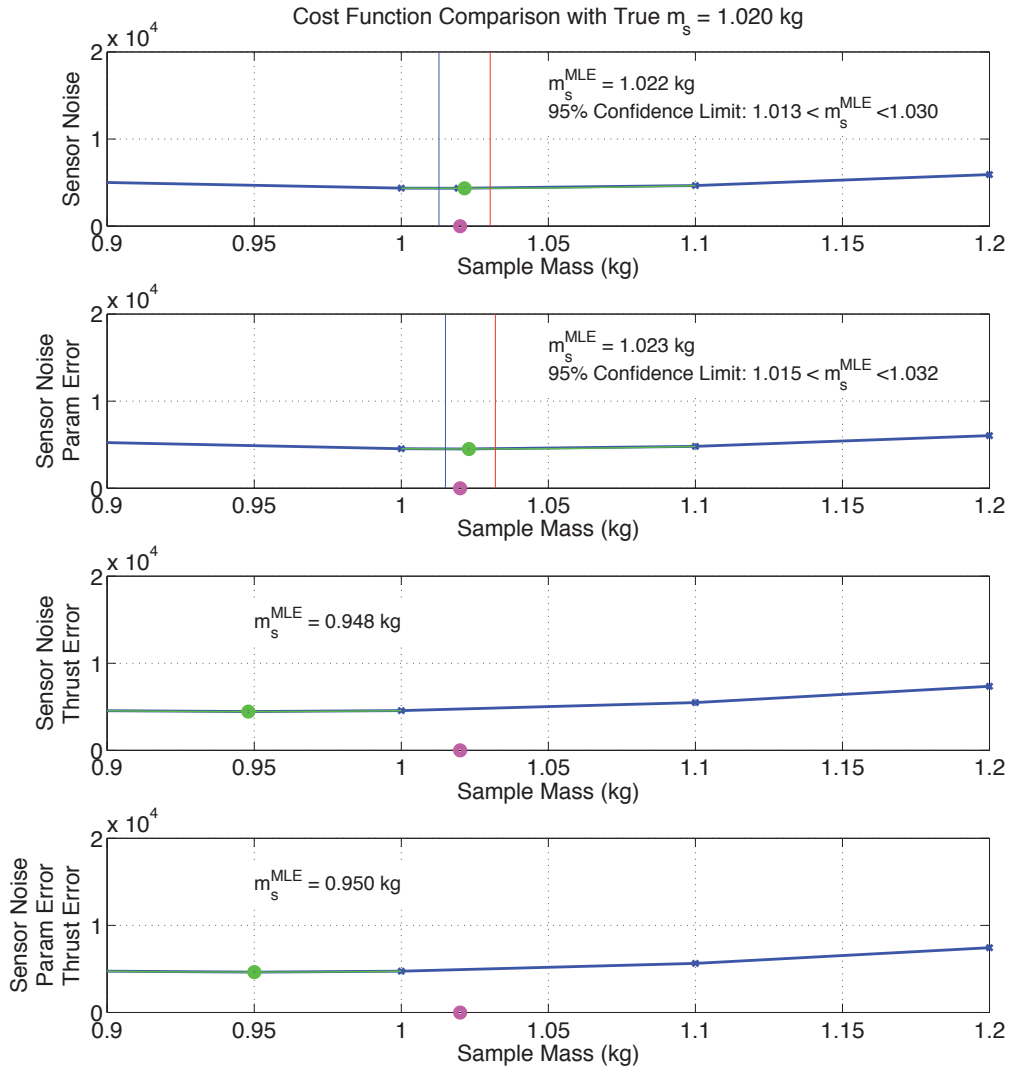

Figure 11: Comparison of Cost and m_s^{MLE} from Different Errors

6 Sample-Mass Estimation Error Budget

For convenience to future missions, a sample-mass estimation error budget is developed from the results of the G-SAMPLE analysis.

6.1 Error Budget Description

The estimate analysis in section 5.2 indicates that noise floor and data sample rate proportionally affect mass estimates and confidence limits. The sensitivity analysis in section 5.3 shows $\pm 10\%$ parametric errors in inertias, center-of-mass offset, and first-flexible mode have little to no effect on the statistics. In contrast, thrust profile errors dominate the sensitivity in G-SAMPLE. These results make up the error budget illustrated in figure 12 for sample mass estimation.

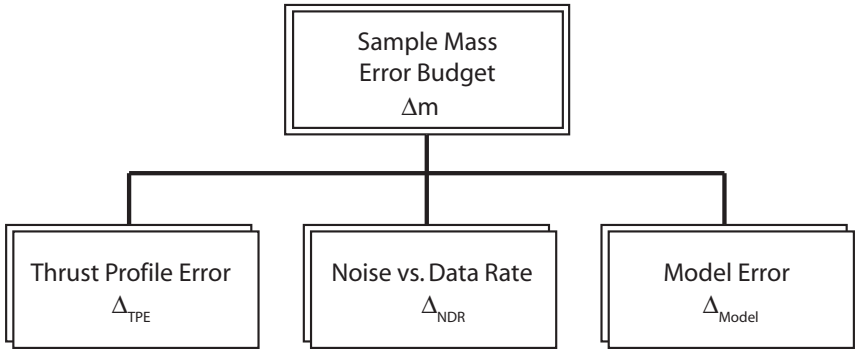

Figure 12: Contributions to Sample-Mass-Estimate Error Budget

The error budget in figure 12 is described by the following equation:

$$\Delta m = \underbrace{\Delta_T m_s}_{\Delta_{TPE}} + \underbrace{\frac{k_{lc}\sigma_{lc}}{|a_{lc}|\sqrt{N}}}_{\Delta_{NDR}} + \Delta_{Model} \tag{66}$$

where m_s is the actual sample mass, Δ_{Model} is the lumped model error ($\Delta_{Model} = 5$ grams is conservative for a wide range of mission scenarios, based on the analysis in section 5.3), k_{lc} is the stiffness of the load sensor in units of N/m, and σ_{lc} is the load-sensor 1-sigma noise level in units of meters. Parameter $|a_{lc}|$ is the sample-mass acceleration in units of m/s^2, and N is number of data samples during a thruster firing. Parameter Δ_T is the thrust profile error (10% thrust error is $\Delta_T = 0.1$). Note, for actual thrust less than expected thrust, estimated sample mass is less than actual; likewise, actual thrust higher than expected makes mass estimates higher than actual mass. Appendix B provides the derivation and assumptions comprising the error budget equation (66).

Figure 13 summarizes representative vertical-thrust T_{vert} versus $|a_{lc}|$ to provide an idea of the magnitude of these quantities; this data comes from simulations of the G-SAMPLE dynamics with spacecraft parameters based on Table 1 in section 5.1. The value of T_{vert} accounts for thruster canting relative to the local vertical. Notice that the relationship is close to linear; this linear relationship is included within the plot.

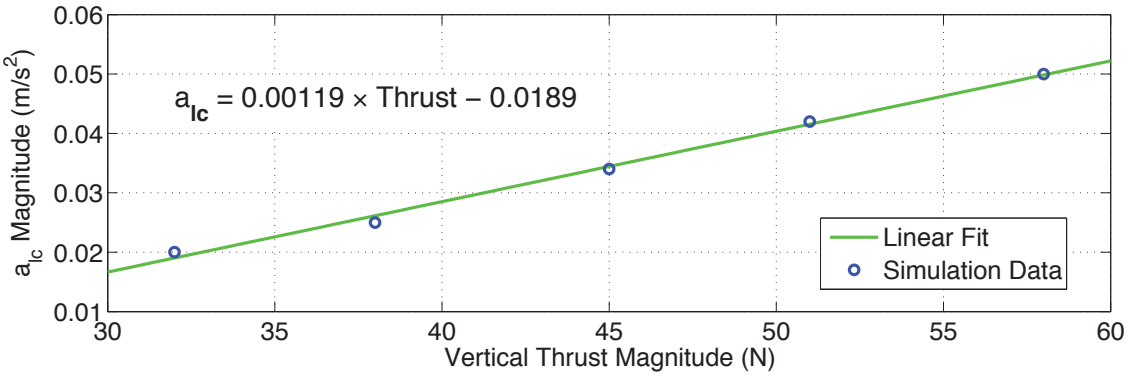

Figure 13: Vertical Thrust and Load-Sensor Acceleration Responses

6.2 Error Budget Example

The following will illustrate an error budget calculation with equation (66) for an expected sample mass of $m_s = 1.02$ kg. During a 10-second ascent thruster firing, with $T_{vert} = 58$ N, the value of $|a_{lc}|$ from Figure 13 is 0.05 m/s^2. A data sample rate of 50 Hz provides $N = 500$ samples during the thruster firing. For a noise floor (including both sensor noise and quantization error) of $\sigma_{lc} = 50\mu$m, the NDR ("Noise vs. Data Rate") contribution to the error budget is

$$\Delta_{NDR} = \frac{k_{lc}\sigma_{lc}}{|a_{lc}|\sqrt{N}} = \frac{\left(250\frac{\mathrm{N}}{\mathrm{m}}\right)\left(50\times10^{-6}\mathrm{m}\right)}{\left(0.05\frac{\mathrm{m}}{\mathrm{sec}^2}\right)\left(\sqrt{500}\right)} = 0.011 \text{ kg} \tag{67}$$

where the value of k_{lc} comes from Table 2 in section 5.1. When the actual thrust profile is 10% below the expected thrust (i.e. $\Delta_T = 0.1$) , the TPE ("Thrust Profile Error") contribution to the error budget is

$$\Delta_{TPE} = \Delta_T m_s = 0.1 \cdot 1.02 \text{ kg} = 0.102 \text{ kg}. \tag{68}$$

As stated earlier, the model error contribution to the budget error is minor, and a conservative value of

$$\Delta_{Model} = 0.005 \text{ kg} \tag{69}$$

is assumed. These contributions provide a total, expected sample error of no more than

$$\Delta m = \Delta_{TPE} + \Delta_{NDR} + \Delta_{Model} = 0.118 \text{ kg}. \tag{70}$$

This offset indicates sample-mass estimates will be below the actual sample mass since actual thrust is 10% below expected thrust. So based on the error budget analysis, the estimate of sample mass will be $m_s^{estimate} = 0.902$ kg.

This case example was run through the G-SAMPLE algorithm where the full nonlinear dynamics model and the G-SAMPLE estimator are used to find the MLE (maximum-likelihood estimate) for collected sample mass. The G-SAMPLE algorithm estimates the collected sample at $m_s^{MLE} = 0.95$ kg, as shown for this case in the bottom plot of figure 11 in section 5.3. The G-SAMPLE estimate differs from the actual sample mass by only 0.07 kg; thus, the error budget equation (66) provides a conservative bound on the error.

7 Conclusions

G-SAMPLE has been developed as a method for in-flight sample mass determination using purely dynamical models with onboard sensor measurements. The use of purely dynamical methods avoids the added expense of cameras or additional sensors for sample mass determination. Simulations utilizing the G-SAMPLE algorithm demonstrate that information from accelerations induced in a typical small-body ascent scenario is suitable to perform an in-flight dynamical estimate of the collected sample mass. For instance, in one example incorporating realistic error assumptions a 1000 gram sample mass is estimated within 110 grams (95% confidence).

The sensitivity of G-SAMPLE is minimal to realistic knowledge errors in actual spacecraft parameters such as inertia, center-of-mass offset, and first flexible mode. However, thrust profile knowledge is shown to be a dominating sensitivity that enters in a nearly one-to-one relationship with the final mass estimation error (i.e. a 10% thrust profile error is effectively a 10% sample-mass

estimate error). This emphasizes that thrust profiles should be well characterized with onboard accelerometers prior to sample collection.

For convenience, results are summarized in a sample-mass estimation error budget that incorporates the sensitivity, noise, and sample rate effects on G-SAMPLE estimates. This error budget provides a simple method to estimate a conservative bound on the sample-mass estimation error that can be used in sample-collection mission proposals and design.

Acknowledgments

I gratefully acknowledge Dr. David S. Bayard of JPL for his guidance in the development of G-SAMPLE and for his contribution of Appendix A to this document. Further, I would like to thank Drs. Behçet Açıkmeşe and Marco Quadrelli of JPL for their valuable comments and suggestions in dynamics modeling. Finally, I would like to thank Michael E. Lisano, Mark S. Wallace, Matthew A. Orzewalla, and Michael B. Meacham for their assistance in developing a representative spacecraft configuration for using in the analysis of G-SAMPLE.

This research was carried out at the Jet Propulsion Laboratory, California Institute of Technology, under a contract with the National Aeronautics and Space Administration, and funded through the internal Research and Technology Development program.

A Appendix: Confidence Limits

Define the measurement sequence as,

$$z_k = y_k(\theta) + n_k, \quad k = 1, ..., N \tag{A.71}$$

where $\theta \in R^p$ and,

$$n_k \sim N(0, \sigma_k^2), \quad k = 1, ..., N \tag{A.72}$$

Then the likelihood function for a single measurement is given by,

$$p(z_k|\theta) = \frac{1}{\sqrt{2\pi}\sigma_k} exp\{-\frac{1}{2}\frac{\big(z_k - y_k(\theta)\big)^2}{\sigma_k^2}\} \tag{A.73}$$

Let $Z^k = \{z_1, z_2, ..., z_N\}$ denote the collection of N such measurements. Assuming the measurements z_k are statistically independent, the likelihood function becomes,

$$p(Z^N|\theta) = \prod_{k=1}^{N} p(z_k|\theta) \tag{A.74}$$

Taking the log of (A.74) and substituting (A.73) gives,

$$L(\theta) \stackrel{\Delta}{=} log\big(p(Z^N|\theta)\big) \tag{A.75}$$

$$= log(\prod_{k=1}^{N} p(z_k|\theta)) = \sum_{k=1}^{N} log(p(z_k|\theta)) \tag{A.76}$$

$$= const - \frac{1}{2}\sum_{k=1}^{N} \frac{\big(z_k - y_k(\theta)\big)^2}{\sigma_k^2} \tag{A.77}$$

Define the maximum likelihood estimate θ^{MLE} as the value of θ that maximizes $L(\theta)$, i.e.,

$$\theta^{MLE} = \arg\max_{\theta} L(\theta) \tag{A.78}$$

Analytically, θ^{MLE} can be found by setting the calculus derivative of $L(\theta)$ to zero, i.e.,

$$\frac{\partial L(\theta)}{\partial \theta} = 0 \tag{A.79}$$

Now consider a Taylor expansion on the log-likelihood function $L(\theta)$ about θ^{MLE},

$$L(\theta) \simeq L(\theta^{MLE}) + \frac{\partial L(\theta)}{\partial \theta}(\theta - \theta^{MLE}) + \frac{1}{2}(\theta - \theta^{MLE})^T \left[\frac{\partial^2 L(\theta)}{\partial \theta \partial \theta^T}\right](\theta - \theta^{MLE}) \tag{A.80}$$

A well-known result [4] is that the MLE estimate becomes asymptotically normal with covariance given by,

$$P = Cov[\theta - \theta^{MLE}] = -\left[\frac{\partial^2 L(\theta)}{\partial \theta \partial \theta^T}\right]^{-1} \tag{A.81}$$

Substituting (A.79) and (A.81) into (A.80)gives,

$$L(\theta) \simeq L(\theta^{MLE}) - \frac{1}{2}(\theta - \theta^{MLE})^T P^{-1}(\theta - \theta^{MLE}) \tag{A.82}$$

which can be rearranged to give,

$$2\big(L(\theta^{MLE}) - L(\theta)\big) = (\theta - \theta^{MLE})^T P^{-1}(\theta - \theta^{MLE}) \tag{A.83}$$

From the asymptotic normality result (A.81), the quantity $\theta - \theta^{MLE}$ can be written as,

$$(\theta - \theta^{MLE}) = P^{\frac{1}{2}} x \tag{A.84}$$

where $P = P^{\frac{1}{2}} P^{\frac{T}{2}}$ and the random vector x is chosen from a standard Gaussian distribution $x \sim N(0, I)$. Consequently, one can has the relationship,

$$(\theta - \theta^{MLE})^T P^{-1}(\theta - \theta^{MLE}) = x^T x \tag{A.85}$$

Since the quantity on the left is the sum of the squares of p independent Gaussians, it is known to be distributed as a $\chi^2(p)$ variate (i.e., Chi-Squared with p degrees of freedom - see the Fisher-Cochrane theorem [5]). Consequently, the right hand side of (A.83) is distributed as a Chi-Squared distribution with p degrees of freedom. As such, the $\%(\alpha \times 100)$ confidence bounds on θ is given by the region satistfying,

$$2\big(L(\theta^{MLE}) - L(\theta)\big) < q(\alpha) \tag{A.86}$$

where $q(\alpha)$ is the α quantile of the Chi-Squared distribution with p degrees of freedom. Note that if sample mass is the only parameter being estimated in the current application, then $p = 1$.

As a further simplication, define the quadratic cost function,

$$J(\theta) \triangleq \sum_{k=1}^{N} \frac{\big(z_k - y_k(\theta)\big)^2}{\sigma_k^2} \tag{A.87}$$

Then by (A.77) one can write,

$$L(\theta) = const - \frac{1}{2} J(\theta) \tag{A.88}$$

Consequently, θ^{MLE} can be found be minimizing $J(\theta)$ rather than maximizing $L(\theta)$. Substituting (A.88) into (A.86) gives the equivalent confidence bounds in terms of $J(\theta)$,

$$J(\theta) - J(\theta^{MLE}) < q(\alpha) \tag{A.89}$$

B Appendix: Error Budget Formulation

B.1 Thrust Profile Error

The TPE (Thrust Profile Error) is based on a $F = ma$ heuristic for the expected force F_{exp} during a fixed acceleration $\bar{a}$. In this formulation, F_{exp} cannot be measured directly, as is the case for thrust or any force. The equations are as follows:

$$F_{exp} = m_s \bar{a} \tag{B.90}$$

$$F_{actual} = m_s a_{actual} \tag{B.91}$$

where $F_{actual} = (1+\Delta_T)F_{exp}$ and $a_{actual} = (1+\Delta_{actual})\bar{a}$. Here, a_{actual} would represent a measured acceleration, which might differ from the desired $\bar{a}$. Then,

$$(1 + \Delta_T)F_{exp} = (1 + \Delta_{actual})m_s\bar{a}$$

$$\implies \Delta_T = \Delta_{actual}$$

and so

$$\Delta_T F_{exp} = (\Delta_T m_s)\bar{a}. \tag{B.92}$$

Then for the actual fixed acceleration $\bar{a}$, the error in the collected sample can be budgeted, based on an assessment of the error in the thrust profile. So the contribution of TPE to the sample-mass error budget is

$$\Delta_{TPE} = \Delta_T m_s. \tag{B.93}$$

B.2 Noise vs. Data Rate Error

The NDR (Noise vs. Data Rate) error contribution is based on a least-squares estimate [6] of simplified load-sensor dynamics where noise enters through the sensor displacement:

$$F_{lc} = m_s a_{lc} = k_{lc} d \tag{B.94}$$

where d is affected by additive zero-mean, Gaussian-white noise $\eta \in \mathcal{N}(0, \sigma_{lc}^2)$ with variance σ_{lc}^2:

$$d = \bar{d} + \sigma_{lc} \cdot \eta. \tag{B.95}$$

In (B.94), measurements of acceleration a_{lc} are assumed to be known perfectly, without contributing noise. A reformulation of (B.94) gives

$$\bar{d} = m_s \bar{a} + v \tag{B.96}$$

where $v = \sigma_{lc} \cdot \eta$ and $\bar{a} = \frac{a_{lc}}{k_{lc}}$. Note, the sign of v is insignificant since η will take on random positive or negative values.

A least-squares estimate $\hat{m}_s$ of the sample mass m_s is given by the following [6]:

$$\hat{m}_s = (A^T A)^{-1} A^T B \tag{B.97}$$

where $A = (\bar{a}_1, \bar{a}_2, ..., \bar{a}_N)^T$ and $B = (\bar{d}_1, \bar{d}_2, ..., \bar{d}_N)^T$ are vectors containing N independent measurements (samples) of $\bar{a}$ and $\bar{d}$, respectively.

The variance of the estimate $\hat{m}_s$ is given by

$$\sigma_m^2 = (A^T A)^{-1} \sigma_{lc}^2. \tag{B.98}$$

If the acceleration $\bar{a}$ is held constant, then this variance can be expressed as follows:

$$\sigma_m^2 = \frac{\sigma_{lc}^2}{N^2 \bar{a}^2} = \frac{k_{lc}^2 \sigma_{lc}^2}{N^2 a_{lc}^2}. \tag{B.99}$$

The standard deviation σ_m represents the contribution of NDR error to the error budget:

$$\Delta_{NDR} = \frac{k_{lc}\sigma_{lc}}{|a_{lc}|\sqrt{N}}. \tag{B.100}$$

References

[1] H. Baruh. *Analytical Dynamics*. McGraw-Hill, 1999.

[2] F.L. Lewis, C.T. Abdallah, and D.M. Dawson. *Control of Robot Manipulators*. Macmillan, 1993.

[3] W.H. Press, B.P. Flannery, S.A. Teukolsky, and W.T. Vetterling. *Numerical Recipes: The Art of Scientific Computing*. Cambridge, 1986.

[4] H.W. Sorenson. *Parameter Estimation: Principles and Problems*. Marcel Dekker, 1980.

[5] G.C. Goodwin and R.L.Payne. *Dynamic System Identification: Experiment Design and Data Analysis*. Academic Press, 1977.

[6] A. Gelb. *Applied Optimal Estimation*. MIT Press, 1974.